Influence of the nature of the gas phase on the degradation of RNA during fossilization processes

J.-C. Viennet, Sylvain Bernard, C. Le Guillou, P. Jacquemot, L. Delbes, E. Balan, M. Jaber

Influence of the nature of the gas phase on the degradation of RNA during fossilization processes

J.-C. Viennet[1,2*], S. Bernard[2], C. Le Guillou[3], P. Jacquemot[1,2], L. Delbes[1], E. Balan[1], M. Jaber[2]

[1]*Muséum National d'Histoire Naturelle, Sorbonne Université, CNRS, UMR 7590, Institut de Minéralogie, Physique des Matériaux et Cosmochimie, Paris, France.*
[2]*Laboratoire d'Archéologie Moléculaire et Structurale, CNRS UMR 8220, Institut des Matériaux de Paris, Sorbonne Université, F-75005, Paris, France.*
[3]*Univ. Lille, CNRS, INRA, ENSCL, UMR 8207 - UMET - Unité Matériaux et Transformations, F-59000 Lille, France*

*Corresponding author J.-C. Viennet, e-mail: jean.christophe.viennet25@gmail.com

Keywords: Biosignatures, Fossilization, RNA world, Clay Minerals, Gas Phase

Highlights:

- The composition of the gas phase impacts fossilization processes.
- Organic compounds are mainly fixed within the interlayer space of the Mg-smectites
- Heterogeneous organo-mineral assemblage could potentially be a biosignature

Abstract

The search for the most ancient traces of life on Earth has always been fraught with controversies because of the inevitable degradation undergone by fossilized biomolecules. Laboratory experiments may provide unique clues to achieve a better mechanistic understanding of the key processes involving (biogenic or abiotic) organic carbon during a geological history. The Earth atmosphere has changed over geological times, from a CO_2-rich atmosphere during the Hadean and Archean to the O_2-rich atmosphere of the present day, with a direct impact on the nature of the gas phase trapped within the sediment porosity. Yet, the influence of the nature of this gas phase on fossilization processes has almost never been investigated. Here, we conducted a series of fossilization experiments using an emblematic biomolecule (e.g. RNA) and clay minerals at 200°C for 7 days in closed systems in equilibrium with two different gas phases (e.g. CO_2 versus N_2/O_2). The multiscale characterization of experimental residues using a suite of advanced microscopy and spectroscopy techniques showed that the final organo-mineral assemblages strongly depend on the nature of the gas phase. In addition to the nature of the mineral phases, results showed that the nature of the gas phase impacts the chemistry of the residual N-rich organic compounds trapped within the interlayer spaces of Mg-smectites (e.g. mainly aliphatic-rich under CO_2 vs dominated by heterocycles under N_2/O_2). Altogether, the present study demonstrates the necessity to take into account the nature of the gas phase composition when experimentally simulating fossilization processes aiming at better constraining which biosignatures may be preserved in ancient rocks. Finally, the experimental results reported here may serve to identify the potential biosignatures that should be searched for on other planetary bodies.

1. Introduction

There is still no consensus on how life originated on Earth nor on what the primordial living cells were (Mann, 2012; Szostak, 2017). Only the fossil record may offer the necessary clues to form a proper appreciation of both the diversity and disparity of ancient life, as well as key information on its origins (Summons & Hallmann, 2014; Knoll *et al.*, 2016). For instance, inspection of the modern biosphere conspicuously fails to anticipate the existence of morphologically curious fossil groups such as Ediacarian biota, trilobites or sauropods (Sereno, 1999; Hughes, 2007; Erwin *et al.*, 2011). The study of the ancient fossil record may thus help better constrain the emergence of primordial life in terms of patterns, rates and processes, as well as the evolution of early terrestrial paleoenvironments.

But this is not that facile. Although the ancient fossil record may contain fundamentally important biogeochemical signals, its poor quality makes it not that easy to decode (McMahon *et al.*, 2018). The search for the earliest traces of life has to take place in the most ancient, and thus disturbed, geological record. Difficulties do not only pertain to the inevitable degradation of fossilized biomolecules occurring during the geological history of their host rocks (Bernard & Papineau, 2014; Briggs & Summons, 2014), but also to the possibility that abiotic chemical pathways yield organic microstructures exhibiting morphological and geochemical signatures very similar to fossilized biogenic ones (Grotzinger & Rothman, 1996; Garcia-Ruiz *et al.*, 2003; Horita, 2005; McCollom & Seewald, 2006; Cosmidis & Templeton, 2016; Rouillard *et al.*, 2018).

Although extrapolating laboratory results to natural settings remains difficult, notably because geological timescales cannot be replicated in the laboratory, fossilization experiments conducted under carefully controlled and reproducible conditions can provide unique clues on the degradation/generation processes of (biogenic or abiotic) organic carbon (Bernard & Papineau, 2014; Javaux, 2019). Of note, such laboratory experiments do not aim at reproducing the full complexity of natural settings (this will never be achieved), but rather aim at creating simple systems to evidence anticipated processes, verify/test thermodynamics predictions or qualitatively and/or quantitatively

investigate the influence of specific parameters.

Following early studies (e.g. Oehler & Schopf, 1971; Oehler, 1976; Briggs & Kear, 1993; Briggs, 1995), many experimental studies have recently been conducted to document the chemical changes of (biogenic or abiotic) organic compounds during a geological history (Ruhl *et al.*, 2011; Schiffbauer *et al.*, 2012; Watson *et al.*, 2012; Li *et al.*, 2013, 2014; McNamara *et al.*, 2013a, 2013b; Fraser *et al.*, 2014; Bernard *et al.*, 2015; Colleary *et al.*, 2015; Picard *et al.*, 2015, 2016; Alleon *et al.*, 2016a, 2017; Miot *et al.*, 2017; Igisu *et al.*, 2018; Saitta *et al.*, 2018; Vinogradoff *et al.*, 2018, 2020). Altogether, these studies highlighted that the degradation of organic molecules can be more abstruse than is generally believed. Besides temperature conditions, these studies documented the influence of the nature of the organic compound, the nature of the mineral matrix and the nature of the fluid on the organo-mineral evolution.

Yet, most of the experiments reported in the literature were conducted using either modern microorganisms or modern biomolecules resistant to fossilization, even though primordial living cells were not as evolved as modern ones and likely did not produce complex resistant macromolecules. In fact, according to the RNA World concept, the primary 'living' substance on the early Earth was RNA (ribonucleic acid) or any compound chemically similar (Hud et al., 2013; Higgs & Lehmann, 2015). Yet, it has long been known that nucleic acids cannot withstand diagenetic conditions (Lindahl, 1993; Levy & Miller, 1998; Mathay *et al.*, 2012), hence drastically limiting the chances of finding preserved fragments within ancient rocks. Conducting fossilization experiments using RNA would offer unique clues on the traces potentially left by the RNA world in the fossil record.

Plus, despite their high potential for biopreservation (e.g. Ehlmann *et al.*, 2008; Summons *et al.*, 2011; Cai *et al.*, 2012; Kennedy *et al.*, 2014; Wacey et *al.*, 2014; McMahon et *al.*, 2018) and despite their continuous formation at the surface of the Earth since the Hadean (Hazen *et al.*, 2008, 2013), smectitic clay minerals have rarely been used in fossilization experiments (Wilson & Butterfield, 2014; McMahon *et al.*, 2016; Naimark *et al.*, 2016; Newman *et al.*, 2019; Viennet *et al.*, 2019a). Because of their ability to adsorb, protect, concentrate, and transform biomolecules, clay minerals such as smectites are believed to have played a major role in the origin of life (Bernal, 1951;

Cairns-Smith, 1966; Hazen *et al.*, 2008, 2013; Meunier *et al.*, 2010; Brack, 2013). Yet the exact impact of clay minerals on biomolecules during fossilization processes remains to be carefully investigated experimentally.

Last, with the exception of experiments conducted by Schiffbauer et al. (2012) which aimed at investigating the effect of redox conditions, the influence of nature of the gas phase has never been investigated. While the exact composition and density of the atmosphere of the early Earth have long been debated (Walker, 1985; Sleep *et al.*, 2001; R. Lowe & Tice, 2004; Tian *et al.*, 2005), it is now widely accepted that it contained no free O_2 and was rather dominated by N_2 and CO_2 (Marty *et al.*, 2013; Kasting, 2014), as suggested by studies of Hadean magmas (Trail *et al.*, 2011). The concentration of CO_2 likely declined from multibar levels during the early Hadean to a few tenths of a bar by the mid- to late Archean (Marty *et al.*, 2013; Kasting, 2014). Such evolution obviously impacted the nature of the gas phase trapped within the sediment porosity. Investigating the influence of the gas phase on the preservation/degradation of molecular biosignatures during advanced fossilization processes thus appears critically needed to properly decode the fossil record.

Here, we experimentally submitted RNA in the presence of Mg-smectites to hydrothermal conditions in pure bi-distilled water at 200°C for 7 days in equilibrium with a gas phase only composed of CO_2 (simulating a primitive atmosphere) or with a gas phase composed of N_2 and O_2 (simulating a modern atmosphere). We characterized the water-insoluble solid residues of experiments at a multiple length scale using X-ray diffraction and advanced spectromicroscopy tools.

2. Materials and methods

2.1. Starting materials

Powder of pure RNA from torula yeast (Sigma-Aldrich) was used for the present experiments. Mg-smectites were synthetized in the lab from a hydrogel of theoretical half-unit-cell formula of saponite: $Na_{0.4}(Mg_3)(Al_{0.4},Si_{3.60})O_{10}(F_{0.05},OH_{0.95})_2$. The hydrogel was obtained by mixing reagents under air

in the following order: pure water, hydrofluoric acid, sodium acetate, magnesium acetate tetrahydrate, aluminium acetate basic and aerosol. The hydrogel was mixed at room temperature for 3 hours and then introduced in a PTFE-lined stainless steel autoclave under air. The autoclave was heated at 220°C for 3 days. After cooling down at room temperature, the Mg-smectites were Ca-saturated by putting in contact 1 $mol.L^{-1}$ of aqueous $CaCl_2$, renewed 5 times, for a total duration of ~60 H. Then, the Ca-saturated Mg-smectites were dried at 60°C after centrifugation within pure water to remove salts. Note that, the initial content of carbon and nitrogen (measured by CHNS elemental analysis see section 2.4.1 below) within the Ca-saturated Mg-smectites are below 0.4 $\%_{Wt}$ and 0.0 $\%_{Wt}$, respectively.

2.2. Fossilization experiments

The fossilziation experiments were conducted in closed system in titanium Parr® reactor of 100 mL at 200°C for 7 days with 1 bar (at 25°C) of a mixture of N_2 and O_2 or 1 bar of pure CO_2. Fifteen mL of pure water were mixed either with 300 mg (±< 0.1%) of Mg-smectites and 150 mg of RNA (± < 0.5%). Pure CO_2 (purity > 99.7%) was flushed into the reactors for 10 min at 20°C. Then the reactor was sealed and heated to 200°C. After 7 days, the sealed reactors were cooled down at ambient temperature. The liquid and solid phases of the residues were separated by centrifugation within pure water before drying at 50°C for ~12 hours. All experiments were triplicated to ensure reproducibility.

2.3. Ultracryomicrotomy

Cryo-ultramicrotome sections (70 nm thick) were prepared for X-ray absorption near edge structure-scanning transmission X-ray microscopy (XANES-STXM) and transmission electron microscopy (TEM) characterization using the Leica ultramicrotome available at UMET (Lille, France). Experimental residues were mixed with 0.1 mL of water-ethanol (50/50 %Vol) before being frozen in liquid nitrogen at -160°C. The sections of frozen residues were then deposited on holey carbon

film TEM grids.

2.4. CHNS estimations

The total carbon and nitrogen contents of the solid fractions of the residues were determined using a Flash 2000 Thermo CHNSO elemental analyser operating at ISTeP (France). About 2 to 3 mg of each residue were combusted under oxygen/helium flux at 960°C. Uncertainties are about 0.02 wt% for N and 0.07 wt% for C.

2.5. X-ray diffraction (XRD)

Powder XRD patterns were obtained on a Panalytical X'pert Pro MPD 2 circles operating at IMPMC (Paris, France), with a step size of 0.033°2θ an a counting time per step of 250s over the 3–65°2θ $CuK\alpha_{1,2}$ angular range. Additional measurements were done using oriented preparations at both atmospheric pressure or under vacuum (3.10^{-4} atmosphere) using an Anton Parr HTK 1200 oven and a temperature monitor TCU1000N coupled to a EDWARDS RV3 pump. The divergence slit, the anti-scatter slit and the two Soller slits were 0.5°, 1°, 0.04° and 0.04 radiant, respectively.

2.6. Fourier-transform infrared (FTIR) spectroscopy

FTIR spectra were recorded over the 400-4000 cm^{-1} range with a 4 cm^{-1} resolution using a Nicolet 6700 FTIR spectrometer fitted with a KBr beamsplitter and a DTGS-KBr detector operating at IMPMC (Paris, France). Spectra were obtained using an attenuated total reflectance (ATR) geometry using a Specac Quest ATR device fitted with a diamond internal reflection element.

2.7. X-ray absorption near edge structure (XANES) spectroscopy

XANES data were collected using the scanning transmission X-ray microscope (STXM) of the HERMES beamline at SOLEIL (Belkhou et al., 2015). Beamline optical elements were exposed to a continuous flow of pure O_2 to remove carbon contamination. Energy calibration was done using the well-resolved 3p Rydberg peak of gaseous CO_2 at 294.96 eV. XANES data were extracted from image stacks collected at energy increments of 0.1 eV over the carbon (270–350 eV) absorption range with a dwell time of ≤ 1 ms per pixel to prevent irradiation damage (Wang et al., 2009). Alignment of images of stacks and extraction of XANES spectra were done using the latest version aXis2000 software (Hitchcock, 2018). The C-XANES spectra shown in the present contribution correspond to homogeneous carbon-rich areas of several hundreds of square nanometers and were normalized to the carbon quantity by integrating the spectra (after subtraction of a power law background) from the pre-edge region up to the mean ionization energy (e.g. 282-291.5 eV at the C K edge) using the QUANTORXS freeware available online (Le Guillou *et al.*, 2018). This freeware also allowed estimating the N/C values of the organic compounds found within the residues, with a precision of ± 0.02 (Alleon *et al.*, 2015).

2.8. Scanning transmission electron microscopy (STEM)

STEM investigations were performed using a Thermofisher Titan Themis 300 microscope operated at 300 keV, located at the “centre commun de microscopie – CCM” at the university of Lille. Hyperspectral EDS data were obtained using the super-X detector system equipped with four windowless silicon drift detectors. These detectors have a high sensitivity for light elements and allow a high counting rate of the carbon, nitrogen and oxygen X-rays. The probe current was set at 600 pA with a dwell time at 10 µs per pixel. The post-processing of the hyperspectral data was performed using Hyperspy (De la Pena *et al.*, 2017). The signal was first denoised using PCA, then fitted by a series of Gaussian functions and a physical model for background/bremsstrahlung. The integrated intensities of the Gaussian functions were used to quantify the compositions thanks to the Cliff-Lorimer method, using experimentally determined k-factors. Absorption correction was taken into

account, which is mandatory to correct for the re-absorption within the sample of the carbon, nitrogen and oxygen X-rays. Finally, end-member phases (smectites, phosphates, amorphous silicon oxides, organic compounds) were identified and their spectra used as inputs for linear combination fitting (multiple linear least square fits). Pixels of similar composition were given the same colors scaled as a function of the proportion of each phase.

3. Results

3.1. Bulk investigations

In the absence of Mg-smectites, the final N/C values of the residues of experiments conducted under N_2/O_2 (0.13) were higher than for those of experiments conducted under CO_2 (0.11) (Table 1). This was similar for residues of experiments conducted in the presence of Mg-smectites (0.18 under N_2/O_2 vs 0.14 under CO_2 – Table 1). In the absence of Mg-smectites, 7.8 wt.% of the initial C and 1.7 wt.% of the initial N were preserved in residues of experiments conducted under CO_2, while 35.4 wt.% of the initial C and 9.4 wt.% of the initial N were preserved in residues of experiments conducted under N_2/O_2 (Table 1). In contrast, in the presence of Mg-smectites, more C and N remained in the residues obtained under CO_2 (i.e. 36.5 wt.% of the initial C and 10.8 wt.% of the initial N under CO_2 versus 20.4 wt.% of the initial C and 7.6 wt.% of the initial N under N_2/O_2) (Table 1).

The XRD patterns of the residues reveal that NH_4^+-rich phosphates formed during the experiments conducted in the absence of Mg-smectites under N_2/O_2 (Fig. 1). In addition, low amounts of Ca-rich phosphates formed under N_2/O_2, while low amounts of Mg hydrated carbonates formed under CO_2. Of note, the Mg and Ca cations came from the pristine RNA salts to compensate the negative charge from the phosphorus backbone. Minor amount of Anatase came from the reactor itself that was released during the residue sampling. During the experiments involving Mg-smectites and RNA, the structure of the Mg-smectites did not evolve that much as indicated by the XRD patterns of the residues (Fig. 1), even though the slight variations of the position and width of the 001 reflection

indicate some disturbance along the c-axis. These residues also contained Al- and Mg-phosphates, whatever the nature of the gas phase (Fig. 1).

None of the residues displayed IR absorption features of RNA (Fig. 2). All the residues of experiments conducted in the absence of Mg-smectites exhibited adsorption bands attributed to CH in alkenes (bands at 983, 930 and 908 cm^{-1}), to CH in alkanes (bands at 1457 and 1374 cm^{-1}), C=O and N-H in amides (bands at 1585, 1680 and 3200 cm^{-}), to CH_2 and CH_3 moieties (bands at 2924, 2860, 2871 and 2960 cm^{-1}, plus the band at 1275 cm-1 for the residues of experiments conducted under N_2/O_2). Of note, residues of experiments conducted under CO_2 exhibited well defined bands corresponding to C-O in alkoxy at 1050, 1100 and 1150 cm^{-1}, while only a large feature centered at 1200 cm^{-1} attributed to C-O in acyl or phenol or alkoxy could be observed for residues of experiments conducted under N_2/O_2. Bands at 740 and 1440 cm^{-1} could be attributed to P-C in aromatic compounds (NIST Office of Data, 2019) while the one at 1014 cm^{-1} for residues of experiments conducted under N_2/O_2 could be attributed to PO_4^{3-} in phosphates.

The Mg-smectites structures of the tetrahedral and octahedral layers did not evolve during the experiments as attested by XRD and FTIR (cf. the Si-O; -OH and Mg_3-OH absorption features at 981, 790; 3675 and 668 cm^{-1}). The formation of phosphates, evidenced by XRD, was confirmed by FTIR (cf. bands at 560 and 600 cm^{-1} attributed to PO_4^{3-} in phosphates). The adsorption band at 1381 cm^{-1} in spectra of residues of experiments conducted under CO_2 were attributed to CO_3^{2-} in carbonates, while the adsorption bands at 1440 and 1560 cm^{-1} corresponded to R-NH_3^+ or NH_4^+ and NH, respectively. In addition, the residues of experiments conducted in the presence of Mg-smectites displayed a band at ~1700 cm^{-1} (more intense for experiments conducted under N_2/O_2), attributed to carboxylic C=O, and bands at 2852, 2928, 2870 and 2960 cm^{-1} (more intense for experiments conducted under CO_2), corresponding to C-H bonds.

3.2. Spatially-resolved investigations

STEM investigations allowed mapping mineralogical heterogeneities within the residues of

281 experiments conducted in the presence of Mg-smectites (Fig. 3). Although Mg-smectites remained
282 the main component of the final residues, Al- and Mg- phosphates were observed, confirming XRD
283 results. In addition, although not detectable using XRD, C-free amorphous Mg,Ca phosphates, C-free
284 amorphous SiO_x particles as well as N-poor organic particles were observed within the residues. The
285 Mg-smectites appeared closely associated with N-rich organic compounds whatever the atmosphere
286 (Fig. 3.B., C. E. and F.), while Ca-carbonates were only observed within residues of experiment
287 conducted under CO_2.

288 STXM-based XANES investigations revealed that RNA was no more present within the
289 residues (Fig. 4.). The XANES spectrum of RNA presents a series of peaks attributed to nucleobases
290 (aromatic and olefinic carbons (285 eV), heterocycles (285.9 eV), ketone and phenol groups (286.7 -
291 287.4 eV)) and ribose (saturated carbons (288 eV) and hydroxyl groups (289.3 eV)) (Le Guillou et
292 al. (2018)) (Fig. 4). The organic residues of experiments conducted in the absence of Mg-smectites
293 appeared very homogeneous and significantly more aromatic than RNA. While under CO_2, RNA
294 evolved into a polyaromatic residue (peak at 285.4 eV attributed to conjugated aromatic cycles –
295 Bernard & Horsfield (2014)), the organic residues of the experiments conducted under N_2/O_2
296 displayed olefinic or aromatic carbons (peak at 285 eV), C=O or C=N or C≡N moieties (peak at 286.7
297 eV) as well as carboxylic groups (peak at 288.4 eV) (Alleon *et al.*, 2017; Vinogradoff *et al.*, 2018).

298 In contrast, the organic fraction of the residues of experiments conducted in the presence of
299 Mg-smectites was heterogeneous (Fig. 4). Despite similar N/C (~ 0.1), the organic compounds
300 associated to the Mg-smectites were not identical in residues of experiments conducted under N_2/O_2
301 and CO_2. Under N_2/O_2 these compounds mainly contained aromatic or olefinic carbons (peak at 285
302 eV), conjugated aromatic cycles (peak at 285.4), heterocycles at 285.8 eV, the compounds that formed
303 under CO_2 mainly exhibited aliphatic carbons (peak at 288 eV) and amide groups (peak at 288.2 eV)
304 with a relatively low amount of aromatic or olefinic carbons (peak at 285 eV). Nanoscale aromatic
305 particles (N/C < 0.05) mainly composed of aromatic and olefinic carbons (peak at 285 eV),
306 conjugated aromatic cycles (285.4 eV) and C=O and C=N groups were observed in the residues
307 whatever the nature of the gas phase.

4. Discussion

4.1. Impact of the nature of the gas phase

The nature of the gas phase (N_2/O_2 vs CO_2) impacted the chemistry of the residues in the absence of Mg-smectites. Although, the N/C values of the solid residues were relatively similar whatever the nature of the gas phase, it was not the case of the final amounts of C and N (Table 1). In fact, the residues of experiments conducted under N_2/O_2 were roughly 5 times richer in C and N than the residues of experiments conducted under CO_2. This was possibly related to the precipitation of NH_4^+-phosphates (that only occurred during the experiments conducted under N_2/O_2) and their P-C bonds preserving the N and C content. The precipitation of such phosphates pinpointed alkaline conditions (Babić-Ivančić *et al.*, 2006; Birnhack *et al.*, 2015) having likely impacted the chemical structure of RNA (cf XANES and FTIR data – Figs. 2 and 4).

Although the aromaticity of the organic fraction increased during all experiments, as expected (Schiffbauer *et al.*, 2012; Li *et al.*, 2014; Bernard *et al.*, 2015; Alleon *et al.*, 2016a, 2017; Vinogradoff *et al.*, 2018; Viennet *et al.*, 2019a), its oxygen content varied with the nature of the gas phase. In fact, the organic fraction of the residues of experiments conducted under N_2/O_2 displayed a higher concentration of oxygen-bearing functional groups, including phenol, alkoxy and amide groups (cf. XANES and FTIR data – Figs. 2 and 4), in good agreement with the experimental study of Schiffbauer et al. (2012).

The nature of the gas phase also impacted the nature of the final residues of the experiments conducted in the presence of Mg-smectites. Besides the precipitation of Ca-carbonates under CO_2 and of Ca-phosphates under N_2/O_2, similar mineral phases formed whatever the nature of the gas phase as a result of the dissolution of Mg-smectites and the degradation of RNA: amorphous silica particles and Al-, Mg- and Mg-Ca-phosphates. Yet, the organic fractions of the residues are different. In contrast to results obtained in the absence of Mg-smectites, the final concentrations of C and N

335 trapped within the solid residues were higher under CO_2, even though the N/C values were slightly
336 higher under N_2/O_2. Of note, an higher amount of residue is obtained under CO_2, as a result of the
337 lower dissolution rate of smectite under CO_2 (Viennet *et al.*, 2017, 2019b).

338 Although the free aromatic-rich particles produced during the experiments were similar
339 whatever the nature of the gas phase, the organic compounds associated to the Mg-smectites were
340 not. This is a quite important point given that these compounds constituted the main organic reservoir
341 of the residues, as confirmed by their N/C values similar to those of the bulk residues. These organic
342 compounds were N-rich within residues of experiments conducted under CO_2 while they were O-rich
343 within residues of experiments conducted under N_2/O_2, in good agreement with the experimental
344 results of Schiffbauer et al. (2012). In fact, other things being equal, Schiffbauer et al. (2012) showed
345 that the presence of oxygen results in a much more aggressive and accelerated degradation of organic
346 compounds. Here, the main driver of the final N/C values was likely the pH. Acidic conditions are
347 known to enhance the thermal degradation of RNA (Matoba et al., 1988), thereby impacting organo-
348 mineral interactions.

349 The organic compounds associated with Mg-smectites might be either adsorbed onto or
350 bonded to surfaces (lateral or basal) or trapped within their interlayer space (Lagaly et al. (2013), and
351 references therein). Exposed to high vacuum (3×10^{-4} atmosphere), the 001 reflections of the
352 experimental residues and of reference Mg-smectites saturated with NH_4^+ exhibited a markedly
353 different behaviour (Fig. 5), attesting that the interlayer space of the Mg-smectites of the residues
354 were full of organic compounds (Ferrage *et al.*, 2005; Gautier *et al.*, 2017; Viennet *et al.*, 2019a). In
355 fact, if no organic compounds were present, the layer to layer distance would have decreased under
356 vacuum as a result of the release of H_2O molecules.

357 XANES and FTIR data revealed that the organic compounds trapped within the Mg-smectites
358 of the residues of experiments conducted under CO_2 were mainly composed of aliphatic carbons and
359 amide groups, suggesting that cationic exchange occurred during the experiments, Ca^{2+} having been
360 replaced by the positively charged organic compounds that efficiently compensated the permanent
361 charge of smectites. In contrast, the organic compounds trapped within the Mg-smectites of the

residues of experiments conducted under N_2/O_2 did not display any amide groups, but rather heterocycles (conjugated or not), carboxylic groups and C=N or N-H bonds. Because they can be positively charged as well, heterocycles such as piperidine or pyrrolidine may have replaced Ca^{2+} within the interlayer space via cationic exchange (Byrne, 1953; Oades & Townsend, 1963; Brindley & Thompson, 1966; Gournis *et al.*, 2004, 2006; Park *et al.*, 2008; Viennet *et al.*, 2019a).

4.2 Implications for decoding the ancient fossil record.

The experimental results reported here have strong implications for our comprehension of the ancient fossil record. Because Archean paleontology relies on imperfect, degraded signals, interpretations have always been and are still, by essence, subject to controversy (Schopf, 1975; Alleon & Summons, 2019). Over the years, many authors have highlighted the equivocal nature of the main criteria used to discuss the biogenicity of putative remnants of life in rocks (Craig, 1954; Buick, 1990; Altermann & Kazmierczak, 2003; Pasteris & Wopenka, 2003; Tice & Lowe, 2004; Awramik & Grey, 2005; Sugitani *et al.*, 2007; Brasier *et al.*, 2015; Wacey *et al.*, 2016, 2018; Rouillard *et al.*, 2018; Alleon & Summons, 2019). With the exception of the recently described objects that have yet to be critically evaluated (Delarue *et al.*, 2017, 2020; Dodd *et al.*, 2017; Hassenkam *et al.*, 2017; Tashiro *et al.*, 2017; Alleon *et al.*, 2018), none of the plethora of 'microfossils' reported from Archean rocks have been fully accepted as authentic biological remains (Schopf, 1975; Alleon & Summons, 2019).

The advanced chemical characterization of ancient potential microfossils using spatially resolved spectroscopy techniques can provide some clues regarding their molecular structure (Javaux & Marshal, 2006; Bernard *et al.*, 2007, 2010; Schiffbauer *et al.*, 2007; Igisu *et al.*, 2009; Steemans *et al.*, 2010; Galvez et al., 2012; Dutta *et al.*, 2013; Alleon *et al.*, 2016b, 2018; Bobroff *et al.*, 2016; Delarue *et al.*, 2017, 2020; Loron *et al.*, 2019; Javaux, 2019), but this is not sufficient to conclude on their biogenicity. In fact, what remains critically missing is information on the original chemical nature of these organic constituents, i.e. information on what these compounds were at the time of

their generation, before the geological history they underwent. Obtaining such information requires the nature and the extent of the transformations that biogenic compounds have undergone since their fossilization to be quantified, i.e. it requires laboratory investigations (Bernard & Papineau, 2014; Briggs & McMahon, 2016; McMahon *et al.*, 2018; Alleon & Summons, 2019; Javaux, 2019).

Many experimental studies investigated the degradation of organic molecules during fossilization processes (cf above), highlighting that it can be quite abstruse, depending on the nature of the organic compound, the nature of the mineral matrix and the nature of the fluid. But, as demonstrated here, special care is needed when conducting laboratory experiments. In fact, most experiments reported in the literature have been conducted either under argon or nitrogen or under the oxygen-rich present day atmosphere. Yet, Schiffbauer et al. (2012) demonstrated that an O_2-rich atmosphere leads to a more aggressive degradation than an inert atmosphere. Worse, the experimental results reported here evidence that the nature of the gas phase impacts the nature of the organic compounds produced during fossilization processes. Given that the Earth atmosphere has changed over geological times, from a CO_2-rich atmosphere during the Hadean and Archean to the O_2-rich atmosphere of the present day (Marty *et al.*, 2013; Kasting, 2014), it definitely appears fundamental to take into account the nature of the gas phase trapped within the sediment porosity (which depends on the composition of the atmosphere to some extent) when experimentally simulating fossilization processes aimed at better constraining which biosignatures may potentially be preserved in ancient rocks.

5. Concluding remarks

The present study highlights the effect of the nature of the gas phase (CO_2 or N_2/O_2) on the thermal degradation (at 200°C and 15.6 bars) of RNA in the presence or absence of Mg-smectites. The organic fractions of the residues of experiments conducted in the absence of Mg-smectites consist in aromatic organic compounds, richer in oxygen and nitrogen under N_2/O_2 than under CO_2. The nature of the gas phase does not impact significantly the nature of the mineral assemblage of residues of experiments conducted in the presence of Mg-smectites. Yet, the N-rich organic compounds fixed

within the interlayer space of the Mg-smectites are dominated by amide groups in residues of experiments conducted under CO_2 gas, while they are dominated by heterocycles such as piperidine or pyrrolidine un residues of experiments conducted under N_2/O_2. Of note, whatever the nature of the gas phase, the organic compounds of the experimental residues did not carry anymore information on the original chemical structure of RNA. Yet, as shown here, the hydrothermal degradation of such a (N,P)-rich organic molecule in the presence of Mg-smectites led to the precipitation of a quite uncommon mineral assemblage comprising submicrometric (Al,Mg,Ca)-phosphates, amorphous silica particles and organic-rich clay minerals (plus Mg-carbonates for experiments conducted under CO_2). Such submicrometric, heterogeneous organo-mineral assemblage could be tentatively seen as a signature of the so-called “RNA world”. Although additional experiments are required to further constrain the impact of fossilization processes, the present experimental results open new avenues for the search for potential biosignatures on other planetary bodies, including rocky and/or icy ones (such as Mars, Ceres, Enceladus or Europa) on which organic compounds, hydrothermal systems and/or N-rich clay minerals have recently been detected (Carter *et al.*, 2013; Ammannito *et al.*, 2016; Carter, 2017; Choblet *et al.*, 2017; Carrozzo *et al.*, 2018; Eigenbrode *et al.*, 2018; Nordheim *et al.*, 2018; Marchi *et al.*, 2019). In other words, there is no doubt that many additional laboratory experiments should be conducted to support astrobiological exploration in eventually providing evidence of the existence of extraterrestrial life.

6. Acknowledgements

The authors wish to acknowledge the workforce of the spectroscopic and X-ray diffraction facilities at IMPMC. Special thanks go to Elisabeth Malassis for administrative simplification, to Stefan Stanescu and Sufal Swaraj for their expert support with the HERMES STXM beamline at SOLEIL, to Anne-Marie Blanchenet for her help during the Cryo-ultramicrotome sections preparations and to François Baudin for his help with CHNS measurements. We gratefully acknowledge financial support from the program Emergences Sorbonne Universités (Project MarsAtLab - PI: S. Bernard) and the DIM MAP (Project FossilEx - PI: M. Jaber and Project BombEx PI: JC. Viennet). The TEM facility

in Lille (France) is supported by the Conseil Régional du Nord-Pas de Calais, and the European Regional Development Fund (ERDF). The HERMES beamline (SOLEIL) is supported by the CNRS, the CEA, the Region Ile de France, the Departmental Council of Essonne and the Region Centre. The authors wish to acknowledge the associated editor Peng Yuan and the anonymous reviewer for their helpful comments.

7. References

Alleon J, Bernard S, Remusat L, Robert F (2015) Estimation of nitrogen-to-carbon ratios of organics and carbon materials at the submicrometer scale. *Carbon* 84, 290–298.

Alleon J, Bernard S, Le Guillou C, Daval D, Skouri-Panet F, Pont S, Delbes L, Robert F (2016a) Early entombment within silica minimizes the molecular degradation of microorganisms during advanced diagenesis. *Chemical Geology* **437**, 98–108.

Alleon J, Bernard S, Le Guillou C, Marin-Carbonne J, Pont S, Beyssac O, McKeegan KD, Robert F (2016b) Molecular preservation of 1.88 Ga Gunflint organic microfossils as a function of temperature and mineralogy. *Nature Communications* 7, 11977.

Alleon J, Bernard S, Le Guillou C, Daval D, Skouri-Panet F, Kuga M, Robert F (2017) Organic molecular heterogeneities can withstand diagenesis. *Scientific Reports* **7**.

Alleon J, Bernard S, Le Guillou C, Beyssac O, Sugitani K, Robert F (2018) Chemical nature of the 3.4 Ga Strelley Pool microfossils. *Geochemical Perspectives Letters* 37–42.

Alleon J, Summons RE (2019) Organic geochemical approaches to understanding early life. *Free Radical Biology and Medicine* 140, 103–112.

Altermann W, Kazmierczak J (2003) Archean microfossils: a reappraisal of early life on Earth. *Research in Microbiology* **154**, 611–617.

Ammannito E, DeSanctis MC, Ciarniello M, Frigeri A, Carrozzo FG, Combe J-P, Ehlmann BL, Marchi S, McSween HY, Raponi A, Toplis MJ, Tosi F, Castillo-Rogez JC, Capaccioni F, Capria MT, Fonte S, Giardino M, Jaumann R, Longobardo A, Joy SP, Magni G, McCord TB, McFadden LA, Palomba E, Pieters CM, Polanskey CA, Rayman MD, Raymond CA, Schenk PM, Zambon F,

Russell CT (2016) Distribution of phyllosilicates on the surface of Ceres. *Science* **353**, aaf4279.

Awramik SM, Grey K (2005) Stromatolites: biogenicity, biosignatures, and bioconfusion. In: (eds. Hoover RB, Levin GV, Rozanov AY, Gladstone GR). Presented at the Optics & Photonics 2005, San Diego, California, USA, p. 59060P.

Babić-Ivančić V, Kontrec J, Brečević L, Kralj D (2006) Kinetics of struvite to newberyite transformation in the precipitation system MgCl2–NH4H2PO4–NaOH–H2O. *Water Research* **40**, 3447–3455.

Belkhou R, Stanescu S, Swaraj S, Besson A, Ledoux M, Hajlaoui M, Dalle D (2015) HERMES: a soft X-ray beamline dedicated to X-ray microscopy. *Journal of Synchrotron Radiation* 22, 968–979.

Bernal JD (1951) The physical basis of life. Routledge and Paul, London.

Bernard S, Benzerara K, Beyssac O, Menguy N, Guyot F, Brownjr G, Goffe B (2007) Exceptional preservation of fossil plant spores in high-pressure metamorphic rocks. *Earth and Planetary Science Letters* **262**, 257–272.

Bernard S, Benzerara K, Beyssac O, Brown GE (2010) Multiscale characterization of pyritized plant tissues in blueschist facies metamorphic rocks. *Geochimica et Cosmochimica Acta* 74, 5054–5068.

Bernard S, Horsfield B (2014) Thermal Maturation of Gas Shale Systems. *Annual Review of Earth and Planetary Sciences* **42**, 635–651.

Bernard S, Papineau D (2014) Graphitic Carbons and Biosignatures. *Elements* **10**, 435–440.

Bernard S, Benzerara K, Beyssac O, Balan E, Brown Jr. GE (2015) Evolution of the macromolecular structure of sporopollenin during thermal degradation. *Heliyon* **1**, e00034.

Birnhack L, Nir O, Telzhenski M, Lahav O (2015) A new algorithm for design, operation and cost assessment of struvite (MgNH4PO4) precipitation processes. *Environmental Technology* **36**, 1892–1901.

Bobroff V, Chen H-H, Javerzat S, Petibois C (2016) What can infrared spectroscopy do for characterizing organic remnant in fossils? *TrAC Trends in Analytical Chemistry* **82**, 443–456.

Brack A (2013) Clay Minerals and the Origin of Life. In: Developments in Clay Science. Elsevier, pp. 507–521.

Brasier MD, Antcliffe J, Saunders M, Wacey D (2015) Changing the picture of Earth's earliest fossils (3.5–1.9 Ga) with new approaches and new discoveries. *Proceedings of the National Academy of Sciences* **112**, 4859–4864.

Briggs DEG, Kear AJ (1993) Fossilization of Soft Tissue in the Laboratory. *Science* **259**, 1439–1442.

Briggs DEG (1995) Experimental Taphonomy. *Palaios* **10**, 539.

Briggs DEG, Summons RE (2014) Ancient biomolecules: Their origins, fossilization, and role in revealing the history of life: Prospects & Overviews. *BioEssays* 36, 482–490.

Briggs DEG, McMahon S (2016) The role of experiments in investigating the taphonomy of exceptional preservation. *Palaeontology* **59**, 1–11.

Brindley GW, Thompson TD (1966) Clay-organic studies: XI. Complexes of benzene, pyridine, and piperidine 1,3-substituted propanes with a synthetic Ca-fluorhectorite. *Clay Minerals* **6**, 345–350.

Buick R (1990) Microfossil Recognition in Archean Rocks: An Appraisal of Spheroids and Filaments from a 3500 M.Y. Old Chert-Barite Unit at North Pole, Western Australia. *PALAIOS* **5**, 441.

Byrne PJS (1953) Some Observations on Montmorillonite-Organic Complexes. *Clays and Clay Minerals* **2**, 241–253.

Cai Y, Schiffbauer JD, Hua H, Xiao S (2012) Preservational modes in the Ediacaran Gaojiashan Lagerstätte: Pyritization, aluminosilicification, and carbonaceous compression. *Palaeogeography, Palaeoclimatology, Palaeoecology* 326–328, 109–117.

Cairns-Smith AG (1966) The origin of life and the nature of the primitive gene. *Journal of Theoretical Biology* 10, 53–88.

Carrozzo FG, Sanctis MCD, Raponi A, Ammannito E, Castillo-Rogez J, Ehlmann BL, Marchi S, Stein N, Ciarniello M, Tosi F, Capaccioni F, Capria MT, Fonte S, Formisano M, Frigeri A, Giardino

M, Longobardo A, Magni G, Palomba E, Zambon F, Raymond CA, Russell CT (2018) Nature, formation, and distribution of carbonates on Ceres. *Science Advances* **4**, e1701645.

Carter J, Poulet F, Bibring J-P, Mangold N, Murchie S (2013) Hydrous minerals on Mars as seen by the CRISM and OMEGA imaging spectrometers: Updated global view. *Journal of Geophysical Research: Planets* **118**, 831–858.

Carter L (2017) Enceladus: Hot spots on an ice world. *Nature Astronomy* **1**, 0084.

Choblet G, Tobie G, Sotin C, Běhounková M, Čadek O, Postberg F, Souček O (2017) Powering prolonged hydrothermal activity inside Enceladus. *Nature Astronomy* **1**, 841.

Colleary C, Dolocan A, Gardner J, Singh S, Wuttke M, Rabenstein R, Habersetzer J, Schaal S, Feseha M, Clemens M, Jacobs BF, Currano ED, Jacobs LL, Sylvestersen RL, Gabbott SE, Vinther J (2015) Chemical, experimental, and morphological evidence for diagenetically altered melanin in exceptionally preserved fossils. *Proceedings of the National Academy of Sciences* **112**, 12592–12597.

Cosmidis J, Templeton AS (2016) Self-assembly of biomorphic carbon/sulfur microstructures in sulfidic environments. *Nature Communications* **7**, 12812.

Craig H (1954) Geochemical implications of the isotopic composition of carbon in ancient rocks. *Geochimica et Cosmochimica Acta* **6**, 186–196.

De la Pena F, Ostasevicius T, Tonaas Fauske V, Burdet P, Jokubauskas P, Nord M, Sarahan M, Prestat E, Johnstone DN, Taillon J, Jan Caron, Furnival T, MacArthur KE, Eljarrat A, Mazzucco S, Migunov V, Aarholt T, Walls M, Winkler F, Donval G, Martineau B, Garmannslund A, Zagonel L-F, Iyengar I (2017) Electron Microscopy (Big and Small) Data Analysis With the Open Source Software Package HyperSpy. *Microscopy and Microanalysis* **23**, 214–215.

Delarue F, Robert F, Sugitani K, Tartèse R, Duhamel R, Derenne S (2017) Investigation of the Geochemical Preservation of *ca.* 3.0 Ga Permineralized and Encapsulated Microfossils by Nanoscale Secondary Ion Mass Spectrometry. *Astrobiology* **17**, 1192–1202.

Delarue F, Robert F, Derenne S, Tartèse R, Jauvion C, Bernard S, Pont S, Gonzalez-Cano A, Duhamel R, Sugitani K (2020) Out of rock: A new look at the morphological and geochemical

551 preservation of microfossils from the 3.46 Gyr-old Strelley Pool Formation. *Precambrian Research*
552 336, 105472.
553 Dodd MS, Papineau D, Grenne T, Slack JF, Rittner M, Pirajno F, O'Neil J, Little CTS (2017)
554 Evidence for early life in Earth's oldest hydrothermal vent precipitates. *Nature* **543**, 60–64.
555 Dutta S, Hartkopf-Fröder C, Witte K, Brocke R, Mann U (2013) Molecular characterization of
556 fossil palynomorphs by transmission micro-FTIR spectroscopy: Implications for hydrocarbon
557 source evaluation. *International Journal of Coal Geology* **115**, 13–23.
558 Ehlmann BL, Mustard JF, Fassett CI, Schon SC, Head III JW, Des Marais DJ, Grant JA, Murchie
559 SL (2008) Clay minerals in delta deposits and organic preservation potential on Mars. *Nature*
560 *Geoscience* **1**, 355–358.
561 Eigenbrode JL, Summons RE, Steele A, Freissinet C, Millan M, Navarro-González R, Sutter B,
562 McAdam AC, Franz HB, Glavin DP, Archer PD, Mahaffy PR, Conrad PG, Hurowitz JA, Grotzinger
563 JP, Gupta S, Ming DW, Sumner DY, Szopa C, Malespin C, Buch A, Coll P (2018) Organic matter
564 preserved in 3-billion-year-old mudstones at Gale crater, Mars. *Science* **360**, 1096–1101.
565 Erwin DH, Laflamme M, Tweedt SM, Sperling EA, Pisani D, Peterson KJ (2011) The Cambrian
566 conundrum: early divergence and later ecological success in the early history of animals. *Science*
567 *(New York, N.Y.)* **334**, 1091–1097.
568 Ferrage E, Lanson B, Sakharov BA, Drits VA (2005) Investigation of smectite hydration
569 properties by modeling experimental X-ray diffraction patterns. Part I. Montmorillonite hydration
570 properties. *American Mineralogist* **90**, 1358–1374.
571 Fraser WT, Watson JS, Sephton MA, Lomax BH, Harrington G, Gosling WD, Self S (2014)
572 Changes in spore chemistry and appearance with increasing maturity. *Review of Palaeobotany and*
573 *Palynology* **201**, 41–46.
574 Garcia-Ruiz JM, Hyde ST, Carnerup AM, Christy AG, Van Kranendonk MJ, Welham NJ (2003)
575 Self-Assembled Silica-Carbonate Structures and Detection of Ancient Microfossils. *Science* **302**,
576 1194–1197.
577 Galvez ME, Beyssac O, Benzerara K, Bernard S, Menguy N, Cox SC, Martinez I, Johnston MR,

578 Brown GE (2012) Morphological preservation of carbonaceous plant fossils in blueschist
579 metamorphic rocks from New Zealand: Fossil preservation in metamorphic rocks. *Geobiology* 10,
580 118–129.
581 Gautier M, Muller F, Le Forestier L (2017) Interactions of ammonium-smectite with volatile
582 organic compounds from leachates. *Clay Minerals* **52**, 143–158.
583 Gournis D, Georgakilas V, Karakassides MA, Bakas T, Kordatos K, Prato M, Fanti M, Zerbetto F
584 (2004) Incorporation of Fullerene Derivatives into Smectite Clays: A New Family of
585 Organic−Inorganic Nanocomposites. *Journal of the American Chemical Society* **126**, 8561–8568.
586 Gournis D, Jankovič L, Maccallini E, Benne D, Rudolf P, Colomer J-F, Sooambar C,
587 Georgakilas V, Prato M, Fanti M, Zerbetto F, Sarova GH, Guldi DM (2006)
588 Clay−Fulleropyrrolidine Nanocomposites. *Journal of the American Chemical Society* **128**, 6154–
589 6163.
590 Grotzinger JP, Rothman DH (1996) An abiotic model for stromatolite morphogenesis. *Nature*
591 **383**, 423–425.
592 Hassenkam T, Andersson MP, Dalby KN, Mackenzie DMA, Rosing MT (2017) Elements of
593 Eoarchean life trapped in mineral inclusions. *Nature* **548**, 78–81.
594 Hazen RM, Papineau D, Bleeker W, Downs RT, Ferry JM, McCoy TJ, Sverjensky DA, Yang H
595 (2008) Mineral evolution. *American Mineralogist* 93, 1693–1720.
596 Hazen RM, Sverjensky DA, Azzolini D, Bish DL, Elmore SC, Hinnov L, Milliken RE (2013)
597 Clay mineral evolution. *American Mineralogist* 98, 2007–2029.
598 Higgs PG, Lehman N (2015) The RNA World: molecular cooperation at the origins of life.
599 *Nature Reviews Genetics* **16**, 7–17.
600 Hitchcock AP (2018) aXis-2000 is an IDL-based analytical package 2000.
601 Horita J (2005) Some perspectives on isotope biosignatures for early life. *Chemical Geology*
602 **218**, 171–186.
603 Hud NV, Cafferty BJ, Krishnamurthy R, Williams LD (2013) The Origin of RNA and “My
604 Grandfather’s Axe.” *Chemistry & Biology* 20, 466–474.

Hughes N (2007) Fossils: professionals and amateurs can cooperate. *Nature* **445**, 709.

Igisu M, Ueno Y, Shimojima M, Nakashima S, Awramik SM, Ohta H, Maruyama S (2009) Micro-FTIR spectroscopic signatures of Bacterial lipids in Proterozoic microfossils. *Precambrian Research* **173**, 19–26.

Igisu M, Yokoyama T, Ueno Y, Nakashima S, Shimojima M, Ohta H, Maruyama S (2018) Changes of aliphatic C-H bonds in cyanobacteria during experimental thermal maturation in the presence or absence of silica as evaluated by FTIR microspectroscopy. *Geobiology* **16**, 412–428.

Javaux EJ, Marshal CP (2006) A new approach in deciphering early protist paleobiology and evolution: Combined microscopy and microchemistry of single Proterozoic acritarchs. *Review of Palaeobotany and Palynology* **139**, 1–15.

Javaux EJ (2019) Challenges in evidencing the earliest traces of life. *Nature* **572**, 451–460.

Kasting JF (2014) Atmospheric composition of Hadean–early Archean Earth: The importance of CO. In: *Geological Society of America Special Papers*. Geological Society of America, pp. 19–28.

Kennedy MJ, Löhr SC, Fraser SA, Baruch ET (2014) Direct evidence for organic carbon preservation as clay-organic nanocomposites in a Devonian black shale; from deposition to diagenesis. *Earth and Planetary Science Letters* **388**, 59–70.

Knoll AH, Bergmann KD, Strauss JV (2016) Life: the first two billion years. *Philosophical Transactions of the Royal Society B: Biological Sciences* **371**, 20150493.

Lagaly G, Ogawa M, Dékány I (2013) Chapter 10.3 - Clay Mineral–Organic Interactions. In: *Developments in Clay Science*, Handbook of Clay Science (eds. Bergaya F, Lagaly G). Elsevier, pp. 435–505.

Le Guillou C, Bernard S, De la Pena F, Le Brech Y (2018) XANES-Based Quantification of Carbon Functional Group Concentrations. *Analytical Chemistry* **90**, 8379–8386.

Levy M, Miller SL (1998) The stability of the RNA bases: Implications for the origin of life. *Proceedings of the National Academy of Sciences* 95, 7933–7938.

Li J, Benzerara K, Bernard S, Beyssac O (2013) The link between biomineralization and fossilization of bacteria: Insights from field and experimental studies. *Chemical Geology* **359**, 49–

69.

Li J, Bernard S, Benzerara K, Beyssac O, Allard T, Cosmidis J, Moussou J (2014) Impact of biomineralization on the preservation of microorganisms during fossilization: An experimental perspective. *Earth and Planetary Science Letters* **400**, 113–122.

Lindahl T (1993) Instability and decay of the primary structure of DNA. *Nature* 362, 709–715.

Loron CC, François C, Rainbird RH, Turner EC, Borensztajn S, Javaux EJ (2019) Early fungi from the Proterozoic era in Arctic Canada. *Nature* **570**, 232.

Mann S (2012) Systems of Creation: The Emergence of Life from Nonliving Matter. *Accounts of Chemical Research* **45**, 2131–2141.

Marchi S, Raponi A, Prettyman TH, Sanctis MCD, Castillo-Rogez J, Raymond CA, Ammannito E, Bowling T, Ciarniello M, Kaplan H, Palomba E, Russell CT, Vinogradoff V, Yamashita N (2019) An aqueously altered carbon-rich Ceres. *Nature Astronomy* **3**, 140.

Marty B, Alexander CMO, Raymond SN (2013) Primordial Origins of Earth's Carbon. *Reviews in Mineralogy and Geochemistry* **75**, 149–181.

Mathay C, Yan W, Chuaqui R, Skubitz APN, Jeon J-P, Fall N, Betsou F, Barnes M, ISBER Biospecimen Science Working Group (2012) Short-Term Stability Study of RNA at Room Temperature. *Biopreservation and Biobanking* **10**, 532–542.

Matoba, T., Kuchiba, M., Kimura, M., Hasegawa, K., 1988. Thermal Degradation of Flavor Enhancers, Inosine 5′-monophosphate, and Guanosine 5′-monophosphate in Aqueous Solution. *Journal of Food Science* 53, 1156–1159.

McCollom T, Seewald J (2006) Carbon isotope composition of organic compounds produced by abiotic synthesis under hydrothermal conditions. *Earth and Planetary Science Letters* **243**, 74–84.

McMahon S., Anderson R. A., Saupe E. E., Briggs D. E. G. (2016) Experimental evidence that clay inhibits bacterial decomposers: Implications for the preservation of organic fossils. Geology, 44, 867–870.

McMahon S, Bosak T, Grotzinger JP, Milliken RE, Summons RE, Daye M, Newman SA, Fraeman A, Williford KH, Briggs DEG (2018) A Field Guide to Finding Fossils on Mars. *Journal of*

659 *Geophysical Research: Planets* **123**, 1012–1040.

660 McNamara ME, Briggs DEG, Orr PJ, Field DJ, Wang Z (2013a) Experimental maturation of
661 feathers: implications for reconstructions of fossil feather colour. *Biology Letters* **9**, 20130184–
662 20130184.

663 McNamara ME, Briggs DEG, Orr PJ, Gupta NS, Locatelli ER, Qiu L, Yang H, Wang Z, Noh H,
664 Cao H (2013b) The fossil record of insect color illuminated by maturation experiments. *Geology* **41**,
665 487–490.

666 Meunier A, Petit S, Cockell CS, El Albani A, Beaufort D (2010) The Fe-Rich Clay Microsystems
667 in Basalt-Komatiite Lavas: Importance of Fe-Smectites for Pre-Biotic Molecule Catalysis During
668 the Hadean Eon. *Origins of Life and Evolution of Biospheres* **40**, 253–272.

669 Miot J, Bernard S, Bourreau M, Guyot F, Kish A (2017) Experimental maturation of Archaea
670 encrusted by Fe-phosphates. *Scientific Reports* **7**.

671 Naimark E, Kalinina M, Shokurov A, Boeva N, Markov A, Zaytseva L (2016) Decaying in
672 different clays: implications for soft-tissue preservation. *Palaeontology* 59, 583–595.

673 Newman SA, Daye M, Fakra SC, Marcus MA, Pajusalu M, Pruss SB, Smith EF, Bosak T (2019)
674 Experimental preservation of muscle tissue in quartz sand and kaolinite. *Palaios* 34, 437–451.

675 NIST Office of Data (2019) WebBook de Chimie NIST.

676 Nordheim TA, Hand KP, Paranicas C (2018) Preservation of potential biosignatures in the
677 shallow subsurface of Europa. *Nature Astronomy* **2**, 673.

678 Oades JM, Townsend WN (1963) The use of piperidine as an aid to clay-mineral identification.
679 *Clay Minerals Bulletin*, **5**, 177-182.

680 Oehler JH, Schopf JW (1971) Artificial Microfossils: Experimental Studies of Permineralization
681 of Blue-Green Algae in Silica. *Science* **174**, 1229–1231.

682 Oehler JH (1976) Experimental studies in Precambrian paleontology: Structural and chemical
683 changes in blue-green algae during simulated fossilization in synthetic chert. *Geological Society of*
684 *America Bulletin* **87**, 117.

685 Park BJ, Sung JH, Park JH, Choi JS, Choi HJ (2008) Poly(vinyl acetate)/Clay Nanocomposite

686 Materials for Organic Thin Film Transistor Application.
687 Pasteris JD, Wopenka B (2003) Necessary, but Not Sufficient: Raman Identification of
688 Disordered Carbon as a Signature of Ancient Life. *Astrobiology* 3, 727–738.
689 Picard A, Kappler A, Schmid G, Quaroni L, Obst M (2015) Experimental diagenesis of organo-
690 mineral structures formed by microaerophilic Fe(II)-oxidizing bacteria. *Nature Communications* **6**,
691 6277.
692 Picard A, Obst M, Schmid G, Zeitvogel F, Kappler A (2016) Limited influence of Si on the
693 preservation of Fe mineral-encrusted microbial cells during experimental diagenesis. *Geobiology*
694 **14**, 276–292.
695 Lowe DR, Tice M (2004) Geologic evidence for Archean atmospheric and climatic evolution:
696 Fluctuating levels of CO2, CH4, and O2 with an overriding tectonic control. *Geology* **32**.
697 Rouillard J, García-Ruiz J-M, Gong J, Zuilen MA van (2018) A morphogram for silica-witherite
698 biomorphs and its application to microfossil identification in the early earth rock record.
699 *Geobiology* **16**, 279–296.
700 Ruhl ID, Salmon E, Hatcher PG (2011) Early diagenesis of Botryococcus braunii race A as
701 determined by high resolution magic angle spinning (HRMAS) NMR. *Organic Geochemistry* **42**,
702 1–14.
703 Saitta ET, Kaye TG, Vinther J (2019) Sediment-encased maturation: a novel method for
704 simulating diagenesis in organic fossil preservation. Palaeontology 62, 135–150.
705 Schiffbauer JD, Yin L, Bodnar RJ, Kaufman AJ, Meng F, Hu J, Shen B, Yuan X, Bao H, Xiao S
706 (2007) Ultrastructural and Geochemical Characterization of Archean–Paleoproterozoic Graphite
707 Particles: Implications for Recognizing Traces of Life in Highly Metamorphosed Rocks.
708 *Astrobiology* **7**, 684–704.
709 Schiffbauer JD, Wallace AF, Hunter JL, Kowalewski M, Bodnar RJ, Xiao S (2012) Thermally-
710 induced structural and chemical alteration of organic-walled microfossils: an experimental approach
711 to understanding fossil preservation in metasediments: Experimental thermal alteration of
712 microfossils. *Geobiology* **10**, 402–423.

Schopf JW (1975) Precambrian Paleobiology: Problems and Perspectives. *Annual Review of Earth and Planetary Sciences* **3**, 213–249.

Sereno PC (1999) The Evolution of Dinosaurs. *Science* **284**, 2137–2147.

Sleep NH, Zahnle K, Neuhoff PS (2001) Initiation of clement surface conditions on the earliest Earth. *Proceedings of the National Academy of Sciences* **98**, 3666–3672.

Steemans P, Lepot K, Marshall CP, Le Hérissé A, Javaux EJ (2010) FTIR characterisation of the chemical composition of Silurian miospores (cryptospores and trilete spores) from Gotland, Sweden. *Review of Palaeobotany and Palynology* **162**, 577–590.

Sugitani K, Grey K, Allwood A, Nagaoka T, Mimura K, Minami M, Marshall CP, Van Kranendonk MJ, Walter MR (2007) Diverse microstructures from Archaean chert from the Mount Goldsworthy–Mount Grant area, Pilbara Craton, Western Australia: Microfossils, dubiofossils, or pseudofossils? *Precambrian Research* **158**, 228–262.

Summons RE, Amend JP, Bish D, Buick R, Cody GD, Des Marais DJ, Dromart G, Eigenbrode JL, Knoll AH, Sumner DY (2011) Preservation of Martian Organic and Environmental Records: Final Report of the Mars Biosignature Working Group. *Astrobiology* 11, 157–181.

Summons RE, Hallmann C (2014) Organic Geochemical Signatures of Early Life on Earth. In: *Treatise on Geochemistry*. Elsevier, pp. 33–46.

Szostak JW (2017) The Origin of Life on Earth and the Design of Alternative Life Forms. *Molecular Frontiers Journal* **01**, 121–131.

Tashiro T, Ishida A, Hori M, Igisu M, Koike M, Méjean P, Takahata N, Sano Y, Komiya T (2017) Early trace of life from 3.95 Ga sedimentary rocks in Labrador, Canada. *Nature* **549**, 516–518.

Tian F, Toon OB, Pavlov AA, Sterck HD (2005) A Hydrogen-Rich Early Earth Atmosphere. *Science* **308**, 1014–1017.

Tice MM, Lowe DR (2004) Photosynthetic microbial mats in the 3,416-Myr-old ocean. *Nature* **431**, 549–552.

Trail D, Watson EB, Tailby ND (2011) The oxidation state of Hadean magmas and implications for early Earth's atmosphere. *Nature* **480**, 79–82.

Viennet J-C, Bultel B, Riu L, Werner SC (2017) Dioctahedral Phyllosilicates Versus Zeolites and Carbonates Versus Zeolites Competitions as Constraints to Understanding Early Mars Alteration Conditions. *Journal of Geophysical Research: Planets* **122**, 2328–2343.

Viennet J-C, Bernard S, Le Guillou C, Jacquemot P, Balan E, Delbes L, Rigaud B, Georgelin T, Jaber M (2019) Experimental clues for detecting biosignatures on Mars. *Geochemical Perspectives Letters* 28–33.

Viennet J-C, Bultel B, Werner SC (2019b) Experimental reproduction of the martian weathering profiles argues for a dense Noachian CO2 atmosphere. *Chemical Geology* **525**, 82–95.

Vinogradoff V, Bernard S, Le Guillou C, Remusat L (2018) Evolution of interstellar organic compounds under asteroidal hydrothermal conditions. *Icarus* **305**, 358–370.

Vinogradoff V, Le Guillou C, Bernard S, Viennet JC, Jaber M, Remusat L (2020) Influence of phyllosilicates on the hydrothermal alteration of organic matter in asteroids: Experimental perspectives. *Geochimica et Cosmochimica Acta* 269, 150–166.

Wacey D, Saunders M, Roberts M, Menon S, Green L, Kong C, Culwick T, Strother P, Brasier MD (2014) Enhanced cellular preservation by clay minerals in 1 billion-year-old lakes. *Scientific Reports* **4**, 5841.

Wacey D, Saunders M, Kong C, Brasier A, Brasier M (2016) 3.46 Ga Apex chert 'microfossils' reinterpreted as mineral artefacts produced during phyllosilicate exfoliation. *Gondwana Research* **36**, 296–313.

Wacey D, Saunders M, Kong C (2018) Remarkably preserved tephra from the 3430 Ma Strelley Pool Formation, Western Australia: Implications for the interpretation of Precambrian microfossils. *Earth and Planetary Science Letters* **487**, 33–43.

Walker JCG (1985) Carbon dioxide on the early earth. *Origins of life and evolution of the biosphere* **16**, 117–127.

Wang J, Morin C, Li L, Hitchcock AP, Scholl A, Doran A (2009) Radiation damage in soft X-ray microscopy. Journal of Electron Spectroscopy and Related Phenomena 170, 25–36.

Watson JS, Fraser WT, Sephton MA (2012) Formation of a polyalkyl macromolecule from the

767 hydrolysable component within sporopollenin during heating/pyrolysis experiments with
768 Lycopodium spores. *Journal of Analytical and Applied Pyrolysis* **95**, 138–144.
769 Wilson LA, Butterfield NJ (2014) Sediment effects on the preservation of burgess shale-type
770 compression fossils. *Palaios* 29, 145–154.
771

772 **Table caption**

773

774 **Table 1:** Concentrations of carbon and nitrogen within the residues.

Experiments	RNA	RNA-CO_2	RNA-N_2/O_2	Smectite-RNA-CO_2	Smectite-RNA-N_2/O_2
Initial mass of Mg-smectites (mg)	-	-	-	300 (±0.1)	300 (±0.1)
Initial mass of RNA (mg)	-	150	150	150	150
Final mass of residue (mg)	-	7.0	26.6	270	193.2
%wtC (±0.07)	31.6	52.9	63.3	6.4	5.0
Initial mass of C (mg)		47.4	47.4	47.4	47.4
Final mass of C (mg)	-	3.7	16.8	17.3	9.7
% of C preserved		7.8	35.4	36.5	20.4
%wtN (±0.02)	14.9	5.7	8.1	0.9	0.9
Initial mass of N (mg)		22.3	22.3	22.3	22.3
Final mass of N (mg)	-	0.4	2.1	2.4	1.7
% of N preserved		1.7	9.4	10.8	7.6
N/C (±0.02)	0.47	0.11	0.13	0.14	0.18

775

776

Figure captions

Figure 1: Powder XRD patterns of the residues of experiments conducted in the presence or absence of Mg-smectites under N_2/O_2 and under CO_2.

Figure 2: Infrared spectra in the middle range of the residues of experiments conducted in the presence or absence of Mg-smectites under N_2/O_2 and under CO_2.

Figure 3: Spatially resolved characterization of the residues of experiments conducted in the presence of Mg-smectites under N_2/O_2 and under CO_2. a, STEM image of a residue of experiments conducted under CO_2 at 200°C in the presence of Mg-smectites. b-c, Maps of minerals and organic compounds (same area as a.). d, STEM image of a residue of experiments conducted under N_2/O_2 at 200°C in the presence of Mg-smectites. e-f, Maps of minerals and organic compounds (same area as D.).

Figure 4: XANES spectra of organic compounds encountered in the residues. The spectrum of RNA is shown for comparison.

Figure 5: XRD patterns on oriented preparation of NH_4^+ saturated Mg-smectites and of the residues of experiments conducted in the presence of Mg-smectites under N_2/O_2 and under CO_2 at atmospheric pressure and under vacuum.

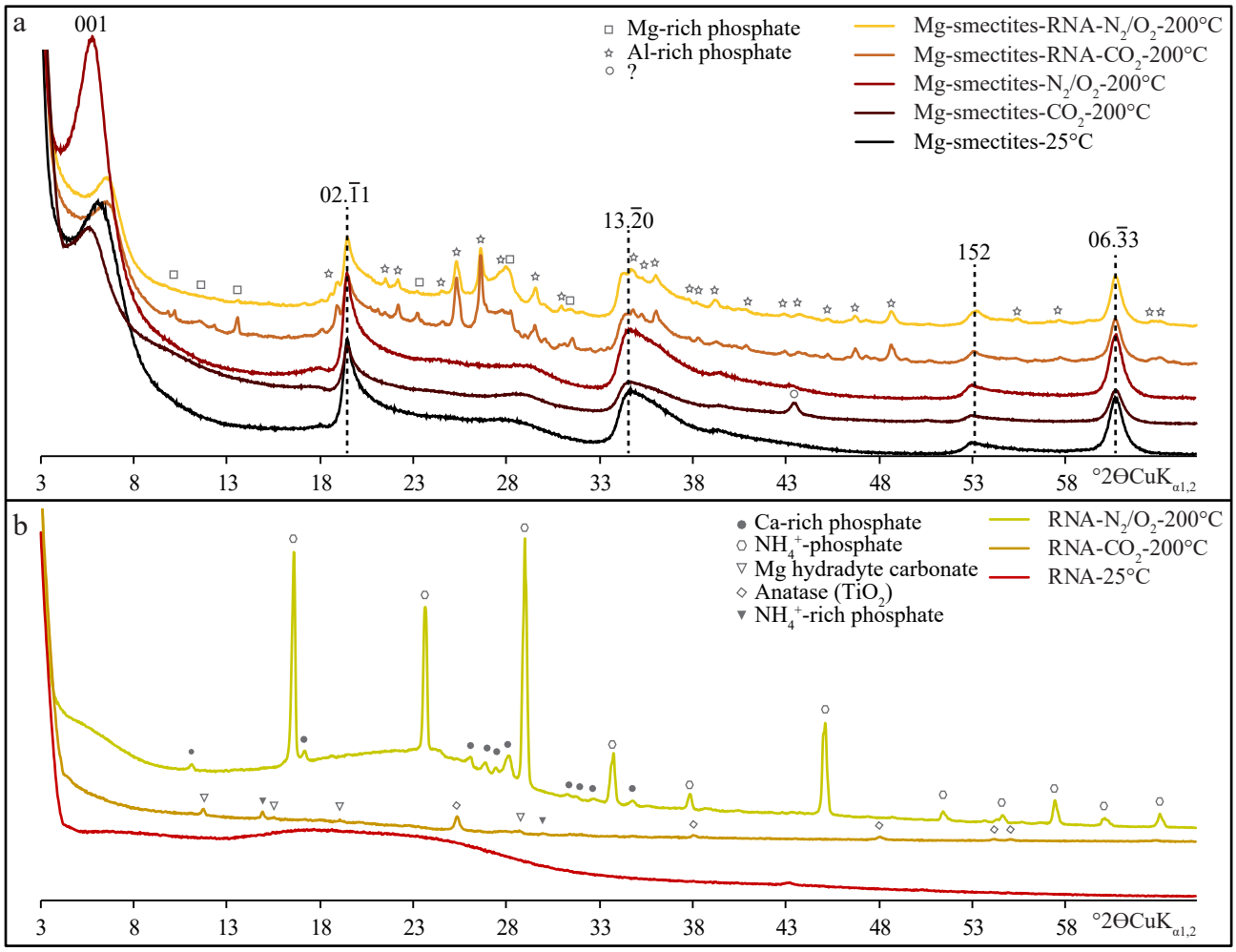
a
001
02.$\bar{1}$1
13.$\bar{2}$0
152
06.$\bar{3}$3
Mg-rich phosphate
Al-rich phosphate
?
Mg-smectites-RNA-N2/O2-200°C
Mg-smectites-RNA-CO2-200°C
Mg-smectites-N2/O2-200°C
Mg-smectites-CO2-200°C
Mg-smectites-25°C
3 8 13 18 23 28 33 38 43 48 53 58 °2ΘCuKα1,2
b
Ca-rich phosphate
NH4+-phosphate
Mg hydradyte carbonate
Anatase (TiO2)
NH4+-rich phosphate
RNA-N2/O2-200°C
RNA-CO2-200°C
RNA-25°C
3 8 13 18 23 28 33 38 43 48 53 58 °2ΘCuKα1,2

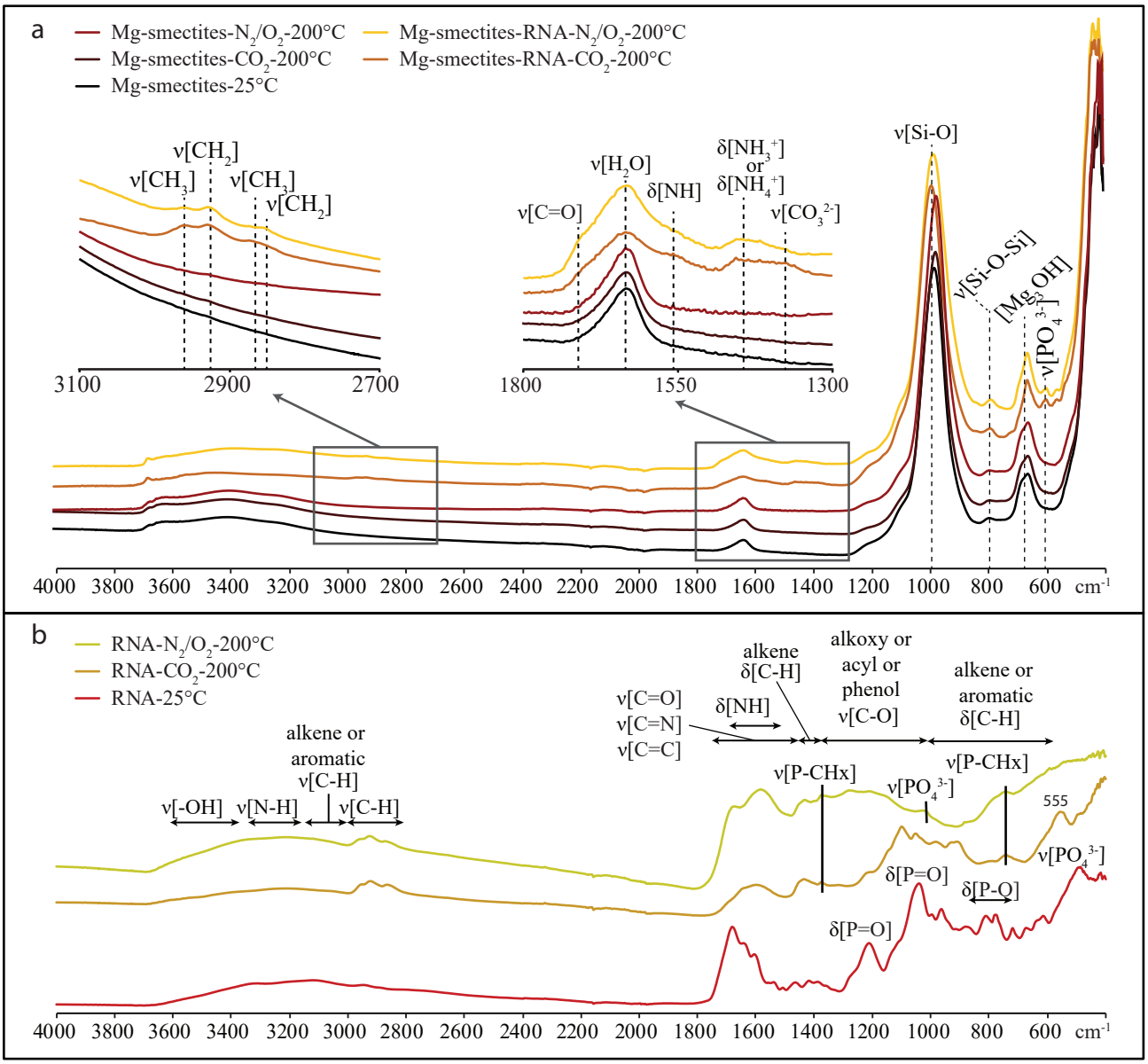
a
Mg-smectites-N2/O2-200°C
Mg-smectites-CO2-200°C
Mg-smectites-25°C
Mg-smectites-RNA-N2/O2-200°C
Mg-smectites-RNA-CO2-200°C
ν[CH2]
ν[CH3]
ν[CH3]
ν[CH2]
3100
2900
2700
ν[H2O]
δ[NH]
δ[NH3+] or δ[NH4+]
ν[C=O]
ν[CO3 2-]
1800
1550
1300
ν[Si-O]
ν[Si-O-Si]
[Mg,Si]-OH
ν[PO4 3-]
4000 3800 3600 3400 3200 3000 2800 2600 2400 2200 2000 1800 1600 1400 1200 1000 800 600 cm-1
b
RNA-N2/O2-200°C
RNA-CO2-200°C
RNA-25°C
alkene or aromatic ν[C-H]
ν[-OH]
ν[N-H]
ν[C-H]
ν[C=O]
ν[C=N]
ν[C=C]
δ[NH]
alkene δ[C-H]
alkoxy or acyl or phenol ν[C-O]
alkene or aromatic δ[C-H]
ν[P-CHx]
ν[PO4 3-]
ν[P-CHx]
555
ν[PO4 3-]
δ[P=O]
δ[P-O]
δ[P=O]
4000 3800 3600 3400 3200 3000 2800 2600 2400 2200 2000 1800 1600 1400 1200 1000 800 600 cm-1

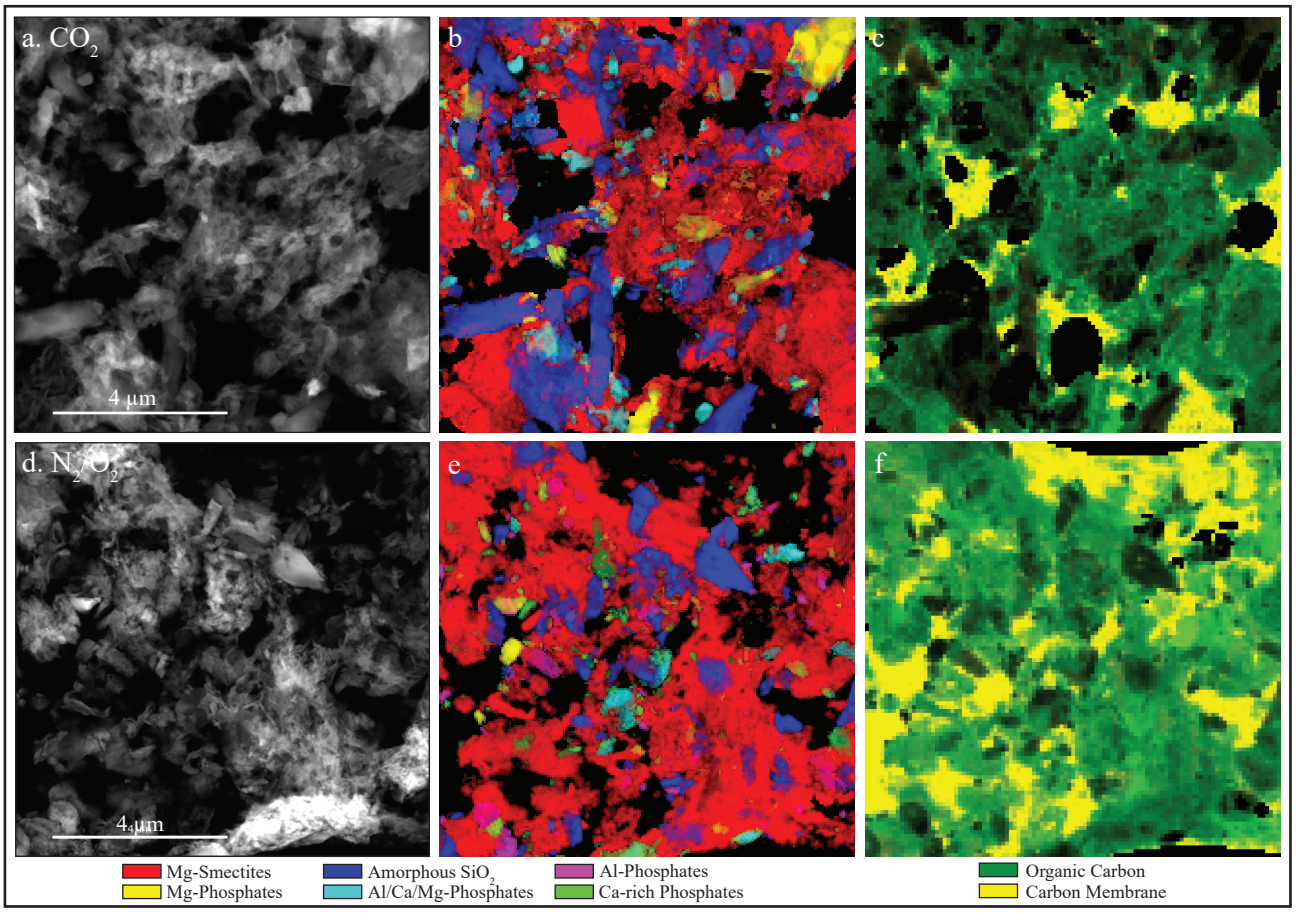
a. CO_2
4 µm
b
c
d. N_2/O_2
4 µm
e
f
Mg-Smectites
Mg-Phosphates
Amorphous SiO_2
Al/Ca/Mg-Phosphates
Al-Phosphates
Ca-rich Phosphates
Organic Carbon
Carbon Membrane

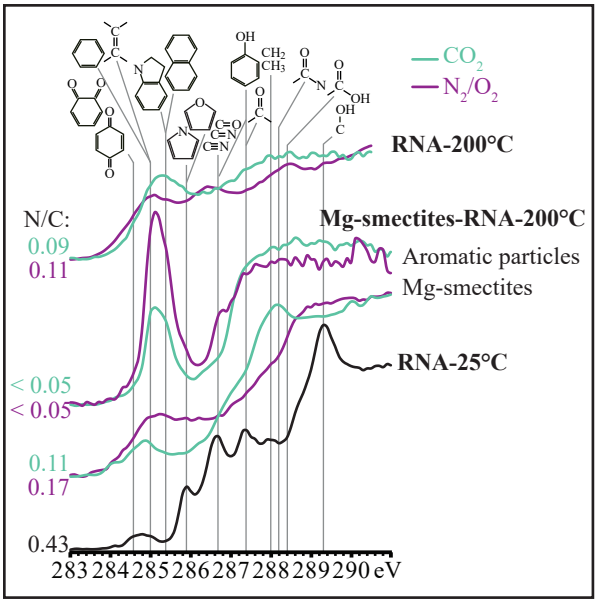
CO2
N2/O2
RNA-200°C
N/C:
Mg-smectites-RNA-200°C
0.09
0.11
Aromatic particles
Mg-smectites
RNA-25°C
< 0.05
< 0.05
0.11
0.17
0.43
283 284 285 286 287 288 289 290 eV

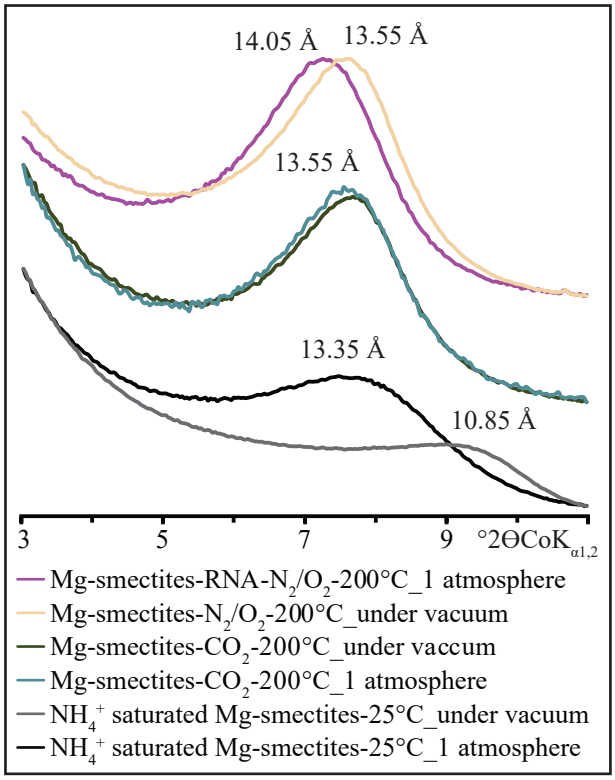
14.05 Å
13.55 Å
13.55 Å
13.35 Å
10.85 Å
3
5
7
9
°2ΘCoK$_{\alpha1,2}$
Mg-smectites-RNA-N$_2$/O$_2$-200°C_1 atmosphere
Mg-smectites-N$_2$/O$_2$-200°C_under vacuum
Mg-smectites-CO$_2$-200°C_under vaccum
Mg-smectites-CO$_2$-200°C_1 atmosphere
NH$_4^+$ saturated Mg-smectites-25°C_under vacuum
NH$_4^+$ saturated Mg-smectites-25°C_1 atmosphere